JOURNAL OF GEOPHYSICAL RESEARCH, VOL. 102, NO. D14, PAGES 16,849–16,859, JULY 27, 1997

Urban/industrial aerosol: Ground-based Sun/sky radiometer and airborne in situ measurements

Lorraine A. Remer,[1] Santiago Gassó,[2] Dean A. Hegg,[2]
Yoram J. Kaufman,[3] and Brent N. Holben[4]

Abstract. Both airborne in situ and ground-based remote sensing methods are used to measure the properties of urban/industrial aerosols during the Sulfate Clouds and Radiation—Atlantic (SCAR-A) experiment in 1993. Airborne in situ methods directly measure aerosol characteristics such as size distribution and scattering coefficient at a particular altitude and infer the total column optical properties, such as optical thickness. Ground-based remote sensing is sensitive to the aerosol optical properties of the entire column and infers the physical properties from inversion of sky radiance. Comparison of optical thickness measurements are encouraging but inconclusive because of measured profiles which extend no higher than 2 km. By comparing aerosol volume size distributions we find that the two systems are in agreement in the radius size range 0.05–2 μm, after the stratospheric aerosol mode is removed from the remote sensing data. At larger aerosol sizes both systems suffer from greater uncertainty, and the larger aerosols themselves are less spatially uniform because of their short lifetimes. The combination of factors makes the comparison at larger radii impossible. The disadvantages of the in situ systems are that there is a measuring efficiency for each device which is dependent on aerosol size and that airborne in situ measurements are rare events in time and space. Also, in situ instruments dry the aerosol before measurement. Automatic remote sensing procedures measure the total column ambient aerosol unaffected by drying or sampling issues, and these instruments can be installed globally to make observations many times per day. However, the disadvantages to remote sensing are that the inferred physical properties are dependent on the assumptions and numerical limitations of the inversion procedures. The favorable comparison between the two types of measurement systems suggests that these drawbacks are manageable in both cases.

1. Introduction

Urban/industrial aerosols created by fossil fuel burning in industrial regions are important variables in the Earth's energy budget [*Charlson et al.*, 1991, 1992; *Kiehl and Briegleb*, 1993; *Mitchell et al.*, 1995]. These aerosols enter into the energy balance either by directly backscattering solar radiation to space (direct effect) [*Charlson et al.*, 1992] or by increasing cloud albedo through microphysical processes (indirect effect) [*Twomey*, 1977, 1984]. In both cases, although the amount of industrial aerosol introduced into the atmosphere each year can be estimated with some accuracy, the quantitative effect of these aerosols on the energy budget and global climate change is largely unknown [*International Panel on Climate Control*, 1994]. Much of this uncertainty is due to our lack of knowledge concerning the physical and optical properties of the aerosols themselves.

There have been many efforts to measure the properties of urban/industrial aerosols using a wide variety of instrumentation. For the purposes of this paper we categorize these methods as either in situ measurements, which measure the aerosol ingested into an instrument system [*Hegg et al.*, 1993a, b; *Leaitch et al.*, 1992; *Hoppel et al.*, 1990], or remote sensing methods, which measure the total column aerosol using either a spaceborne [*Durkee et al.*, 1991] or ground-based radiometer [*King et al.*, 1978; *Kaufman et al.*, 1994; *Kaufman and Fraser*, 1983; *Nakajima et al.*, 1983]. Each method has advantages and disadvantages. For example, in situ measurements at ground level measure only the aerosol within a few meters of the Earth's surface at one location and may not be representative of the mixed aerosol in the total boundary layer. On the other hand, remote sensing of aerosol from spaceborne platforms must decouple the measured radiance signal into its two components: one originating from the Earth's surface and the second originating from the atmosphere [*Holben et al.*, 1992]. In certain cases these disadvantages may be alleviated. Airborne in situ measurements can measure profiles of aerosol properties and sample over a spatially diverse area and thus provide a more comprehensive description of aerosol properties than can be measured at the ground. Ground-based remote sensing of aerosol properties takes advantage of the dark background of space or the constant signal of the solar disk and thereby eliminates the concern of separating the atmospheric component from the background component of the radiance signal. These two methods, airborne in situ measurements and

[1]Science Systems and Applications Incorporated, NASA Goddard Space Flight Center, Greenbelt, Maryland.
[2]Department of Atmospheric Science, University of Washington, Seattle.
[3]Laboratory for Atmospheres, NASA Goddard Space Flight Center, Greenbelt, Maryland.
[4]Laboratory for Terrestrial Physics, NASA Goddard Space Flight Center, Greenbelt, Maryland.

Paper number 96JD01932.
0148-0227/97/96JD-01932$09.00

ground-based remote sensing, provide the most reliable means of determining the optical and physical properties characteristic of the total aerosol column and are the subject of this study.

The Sulfate Clouds and Radiation—Atlantic (SCAR-A) experiment in the mid-Atlantic region of the eastern United States during July 1993 provides a comprehensive database from which to analyze the optical and physical properties of urban/industrial aerosols [*Kaufman and Holben*, 1996; *Remer et al.*, 1996]. During the summer the eastern seaboard typically experiences periods of extremely hazy conditions associated with urban/industrial pollution [*Husar et al.*, 1981]. In situ measurements of the SCAR-A aerosol show that the aerosol is typically composed of sulfates, a marine influence of salt, nitrates, and organics [*Hegg et al.*, 1995]. The experiment employed both airborne in situ measurements by the University of Washington C-131A aircraft and ground-based remote sensing by a network of six automatic spectral Sun/sky scanning radiometers. The University of Washington plane carries an array of instrumentation which measures many meteorological, cloud, and aerosol variables including aerosol concentration, size distribution, extinction, scattering, and composition [*Hobbs et al.*, 1990; *Hegg et al.*, 1993b]. These data can be used to derive aerosol optical thickness. The ground-based radiometer network measured direct solar radiation and sky radiance, which is later processed and inverted to obtain spectral optical thickness, Angstrom wavelength exponent, precipitable water, aerosol phase function, and size distribution [*Holben et al.*, 1996]. Thus, during events when the C-131A was flying above a ground-based radiometer near the time of an observation, the in situ measurements of aerosol optical thickness and aerosol size distribution can be compared to the same quantities inverted from the radiance measured by the radiometer on the ground. Agreement between the two measuring methods will support the validation of both procedures. Disagreements will highlight the limitations inherent in each method. In this study we describe the instrumentation used in both procedures and discuss the advantages and disadvantages of each. We then compare concurrent measurements of aerosol optical thickness and aerosol volume size distributions. We also compare each method's ability to measure the dynamic properties of the sulfate aerosol and discuss the implications on future field campaigns.

2. Airborne in Situ Instrumentation and Data

2.1. Instrument Description

In addition to the standard meteorological and cloud physics parameters measured on a routine basis and described by *Hobbs et al.* [1990], the C-131A carried several distinct measurement systems for the measurement of the aerosol size distribution and the light scattering caused by the aerosol. Data for four of these systems have been utilized in this study, and hence these systems are briefly described here.

The first such system and the simplest in conception is the passive cavity aerosol spectrometer probe (PCASP) manufactured by Particle Measurement Systems (PMS) Incorporated. This probe measures the aerosol size distribution over a nominal range of 0.1–3.0 μm diameter using a pulse height analyzer to bin light pulses scattered by particles illuminated in a laser beam. Calibration of the device was accomplished in the smaller sizes by generating salt particles (both NaCl and $(NH_4)_2SO_4$) by a Coulison atomizer, sizing them with an electrostatic classifier, and aspirating them into the PCASP. The larger channels were checked with glass beads from Duke Scientific. The calibration range of the probe was found to be 0.12–3.0 μm diameter, in essential agreement with the results of *Liu et al.* [1992]. The PCASP was mounted on the aircraft wing, ~2 cm in front of and 0.5 m below the leading edge. An integral diffuser cone decelerated the flow prior to aspiration into the laser beam. Compressional heating in the cone heated the sampled aerosol ~2°C above ambient (determined by direct measurement).

The second system utilized to measure the aerosol size distribution is the batch sampler described by *Radke* [1983] and called the no-bag sampler. It consists of an 80-L stainless steel cylinder with a light weight fiber glass piston which is filled periodically by ram air. After filling, the aerosols in the cylinder are sampled through a diffusion dryer by two sizing instruments, a PMS ASASP-100X and a PMS LAS-200. These instruments, both laser spectrometers similar in conception to the PCASP, sample over the size ranges 0.1–3.0 and 0.5–13.0 μm, respectively. However, because of impaction losses in the inlet and ram air line, the 50% sampling efficiency point of this batch sampler is a nominal 5 μm diameter (airspeed and angle-of-attack dependent). Calibration procedures are similar to those used for the PCASP. It should be noted that the diffusion dryers lower the sampling relative humidity (RH) to ~40%.

The third system utilized in this study is a three-wavelength, integrating nephelometer built in-house at the University of Washington by N. Ahlquist and A. P. Waggoner. The wavelength discrimination is achieved with interference filters of 40-nm bandwidth centered at 450, 550, and 700 nm. Rayleigh scattering is internally calculated (from pressure and temperature sensors in the measurement volume) and subtracted from the particle scattering signal. The device is calibrated using particle free air together with a suite of particle free gases whose scattering efficiencies are well known (e.g., CO_2, SF_6, and F_{12}). Prior to entering the nephelometer the sample air (entrained through a diffuser-capped inlet maintained isokinetic by a vacuum pump) is passed through a heated plenum chamber to dry the air to a nominal 40% RH, for ambient RH < 85%.

The final system employed in the study is the radiance research absorption photometer. This device measured particle light absorption at a nominal wavelength of 530 nm with 5-min time resolution. The technique utilized in the instrument is an automated version of the integrating plate method as discussed by *Weiss and Waggoner* [1984]. As with the nephelometer, the sample air was taken from the heated plenum chamber.

2.2. Humidity Correction

The rationalization for the drying of the ambient aerosol prior to measurement of either the size distribution or the aerosol light-scattering coefficient is the standard one of intercomparability with other measurements. However, because an important aspect of this study is the intercomparison of the in situ measurements with remote retrievals, which characterize the aerosol under ambient conditions, a correction of the size distribution and particularly the light-scattering coefficient to ambient conditions is in order. This has been accomplished by employing literature values for both the dependence of aerosol size [e.g., *Hanel*, 1976; *Svenningson et al.*, 1992] and light-scattering coefficient [e.g., *Covert et al.*, 1972] on relative humidity. Additionally, for the light-scattering coefficient we have also made use of a series of measurements that we have taken in modestly polluted marine air [*Hegg et al.*, 1996] and to

estimates based on closure calculations with the SCAR-A data themselves. The form of the correction for RH, whether for particle size or light scattering, follows that advocated by *Hanel* [1976]. For example, for the aerosol light-scattering coefficient, the magnitudes at any two RHs are related by

$$\frac{\sigma_{sp}(RH_1)}{\sigma_{sp}(RH_2)} = \left(\frac{1 - RH_1}{1 - RH_2}\right)^{-\gamma} \quad (1)$$

where σ_{sp} is the light-scattering coefficient and γ is an empirically determined constant. For spherical particles of uniform composition [*Van de Hulst*, 1957],

$$\sigma_{sp}(z, \lambda) = \int_0^\infty \pi r^2 Q_{scatt}(r, \lambda, m(\lambda)) n(r)\, dr \quad (2)$$

where $n(r)$, measured in $cm^{-3}\ \mu m^{-1}$, is the particle size distribution curve, $Q_{scatt}(r, \lambda, m(\lambda))$ is the Mie scattering efficiency factor for spherical particles of radius r, and $m(\lambda)$ is the complex index of refraction at wavelength λ. Throughout this analysis, Mie algorithms [*Wiscombe*, 1979, 1981] are used to calculate the particle scattering efficiencies. Typical values for γ (for light scattering) under polluted conditions are 0.2–0.5. For particle size, values of γ generally fall in the 0.1–0.3 range.

To narrow the uncertainty for γ in the SCAR-A data, we use a closure calculation in which we compare the directly measured σ_{sp} and a derived σ_{sp} calculated from (2), where $n(r)$ is the PCASP measured size distribution. *Hanel*'s [1976] formula (equation (1)) is used to achieve closure with γ adjusted to produce the best fit to the measured quantity. There are in fact two free parameters: γ and the index of refraction. However, if the aerosol composition is known from filter samples [*Hegg et al.*, 1996], the index of refraction is also known and γ becomes the only free parameter. For several aerosol samples the composition was sufficiently well known (mass closure >90%) to permit such an analysis. From this analysis it was determined that $\gamma = 0.35$ minimizes the error between the measured and calculated scattering coefficients. This value is in agreement with previous measurements [*Hegg et al.*, 1996; *Covert et al.*, 1972]. Nevertheless, the minimization did not result in zero error or difference between calculated and measured coefficients. The remaining differences between measured and calculated coefficients ranged between 1 and 14%, depending on the aerosol parcel studied. These residual errors are partially due to residual uncertainties in the aerosol index of refraction. For example, in the cases examined, sulfate constituted more than 90% of the aerosol mass. However, the molecular form of the sulfate was not determined. The real part of the refractive index could vary from 1.52 (ammonium sulfate) to 1.47 (ammonium bisulfate) resulting in residual differences between observed and calculated scattering coefficient of 10% when γ is held constant.

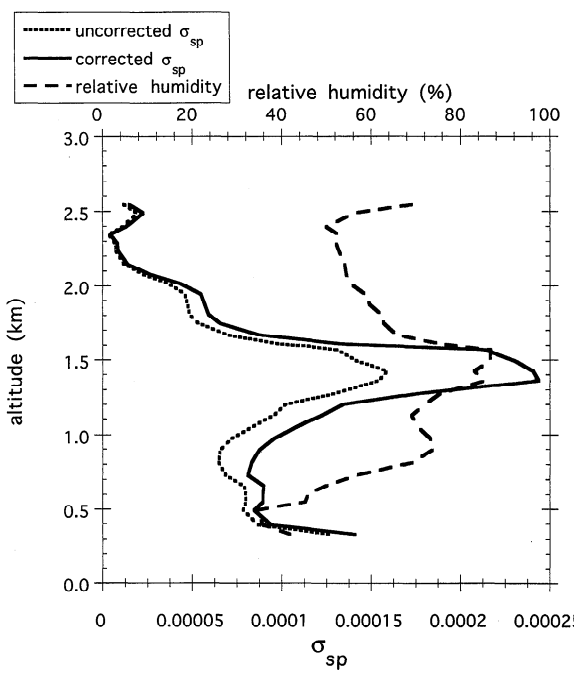

Figure 1. Light-scattering coefficient at 450 nm, σ_{sp} (solid and dotted curves) and relative humidity (dashed curve) plotted as a function of aircraft altitude for an in situ profile taken on July 28. Shown are σ_{sp} measured from the dried sample air (dotted curve) and the values after humidity correction (solid curve), where $\gamma = 0.35$.

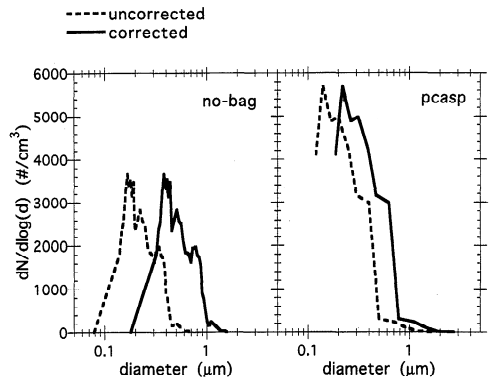

Figure 2. Example of humidity correction on size distribution for $\gamma = 0.30$. Dashed curves represent dry, uncorrected data. Solid curves represent wet, ambient conditions after humidity corrections. Data were collected July 20 in a layer where ambient relative humidity was 96%.

Now that we have determined a value for γ from closure between in situ measurements, we can use this value of γ to correct the in situ measurements of light scattering to ambient conditions. Figure 1 shows an example from one profile taken on July 28. We see that in the layer of high relative humidity at 1400 m the values of σ_{sp} jump from 0.00015 before correction to 0.00025 after correction. The effect of the correction on optical thickness measurements will be discussed in a later section.

To correct particle size, we choose $\gamma = 0.30$ from [*Svenningsson et al.*, 1992; *McMurry and Stolzenburg*, 1989]. Because the PCASP probe measures particles close to ambient relative humidity, the results of the correction will be insensitive to the precise value of γ used. Figure 2 shows an example of the particle size correction using data taken on July 20 when ambient relative humidity was high (96%). Even though the no-bag and PCASP data were taken in the same atmospheric layer, at the same time, they differ in the size and number of particles measured. The uncorrected no-bag size distribution measured at 40% relative humidity peaks at particle diameter approximately 0.17 μm. After correction to ambient conditions the no-bag sample peaks at particle diameter 0.40 μm. The PCASP data are subjected to less drying and therefore less correction. PCASP-measured particle size is corrected from

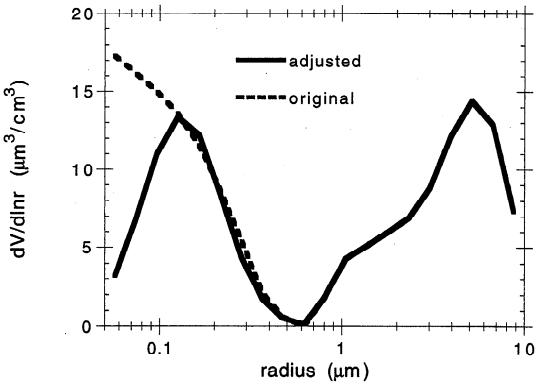

Figure 3. Volume size distribution derived from spectral sky radiance data and inverted using *Nakajima* [1983, 1986] code (dashed curve) and adjusted to better fit the small radius edge (solid curve), using a technique that matches the aerosol single-scattering path radiance of original curve with path radiance of a lognormal size distribution in a look-up table. The lognormal in this case is represented by $r_g = 0.063$ and $\sigma = 0.50$ with a root-mean-square (rms) difference in path radiance of 8%. The data are from an observation on July 28 corresponding to event 6 in Table 2.

0.14 μm (dry) to 0.22 μm (wet). Because the PCASP probe measures particles closer to ambient conditions, it is the preferred instrument to use in comparison with remote sensing data.

3. Spectral Scanning Sun/Sky Radiometer Data

3.1. Instrument Description

The SCAR-A network of Sun/sky radiometers consists of six individual instruments. Each instrument measures solar radiance in six spectral bands (340, 440, 670, 870, 940, and 1020 nm) automatically every 15 min and sky radiance in four spectral bands (440, 670, 870, and 1020) roughly every hour, weather permitting. Data processing of the direct Sun measurements provides spectral aerosol optical thickness, Angstrom wavelength exponent, and precipitable water [*Holben et al.*, 1996]. The sky radiance is measured in the solar almucantar during low Sun angles and in the principal plane during high Sun angles. The almucantar is defined as a plane with a fixed view zenith angle, and the principal plane is defined as a plane with a fixed view azimuth angle that includes the Sun. The almucantar measurements are checked for symmetry of the sky radiance on either side of the Sun, and asymmetrical almucantars are discarded. Asymmetry is due to nonhomogeneous atmospheric conditions or the presence of clouds. The sky radiance data in the first 40° from the solar disk from each symmetrical almucantar are inverted into phase function, volume size distribution, and aerosol optical thickness [*Nakajima et al.*, 1983, 1986]. Sensitivity studies of the almucantar inversion show that volume size distribution retrievals are reasonable for particles with radii between 0.1 and 4.0 μm [*Kaufman et al.*, 1994]. There is no comparable asymmetry check on the principal plane measurements, and the retrievals from the principal plane data have undergone less scrutiny and testing than those from almucantar measurements. For these reasons, the comparisons of size distribution in this study are limited to retrievals from almucantar measurements, which are taken in the morning and late afternoon when the Sun's zenith angle is greater than 60°.

3.2. Volume Size Distribution Retrieval

The *Nakajima et al.* [1983, 1986] inversion technique assumes that beyond the size limits of the inversion (radii of 0.07 and 9 μm) the particle volume is zero. This assumption affects the resulting volume distribution by artificially increasing volume at the size limits of the inversion in order to compensate for the arbitrary and unphysically low volume just beyond the limits. The overcompensation affects both the small- and large-particle edges of the volume size distribution. In this study we concentrate on the small particles because the large-particle volume is less optically important at visible wavelengths and is affected by stray light in the radiometer optics. Also, large particles are not measured as well by the in situ instrumentation aboard the C-131A aircraft because of impaction in the sample line. Furthermore, large particles are more variable in space and time due to their shorter lifetimes and are therefore more difficult to compare in this study. Because of these inherent difficulties in both types of instrumentation and in the nature of the particles themselves, we will find comparisons of large-particle retrieval to be difficult and thus will not spend much time "adjusting" the *Nakajima et al.* [1983, 1986] inversion technique for the overcompensation at the large-particle end. We do adjust the retrieved volume size distribution for the smallest particles in the following manner. Two assumptions are necessary. (1) Even though the inverted volume distribution is in error, the inversion algorithm guarantees that these size distributions do correctly represent the optical properties of the aerosol, and (2) physically, the aerosol will be best represented for small accumulation mode particles by a single lognormal distribution [*Whitby*, 1978; *Hegg et al.*, 1993a; *Hoppel et al.*, 1985, 1990]. The lognormal distribution is defined as

$$\frac{dN}{dr} = \frac{N_0}{\sigma_g r \sqrt{2\pi}} \exp\left(-\frac{[\ln (r/r_g)]^2}{2\sigma_g^2}\right) \tag{3}$$

where dN/dr is the number size distribution, σ_g is the standard deviation of the natural logarithm of the radius, and r_g is the mean modal radius. The adjustment procedure is to input the retrieved number size distribution into a Mie computation code [*Dave and Gazdag*, 1970] in order to recalculate the aerosol single-scattering path radiance $L_p^{\text{obs}}(\theta, \lambda)$ in the first 40°. We then match $L_p^{\text{obs}}(\theta, \lambda)$ to $L_p^{\text{calc}}(\theta, \lambda)$ in a look-up table, where $L_p^{\text{calc}}(\theta, \lambda)$ is the path radiance calculated for single lognormals of various radii and widths. Thus we can find a lognormal with the same optical properties of the inverted size distribution but having a better physical representation. All inverted size distributions shown in this study have been adjusted in the small-particle region by means of matching $L_p^{\text{obs}}(\theta, \lambda)$ in a look-up table. An example of this adjustment is shown in Figure 3.

In the case illustrated in Figure 3 the matched lognormal has $r_g = 0.063$ μm and width 0.50 (corresponding to volume modal radius 0.133 μm). The root-mean-square error (rmse) of the match is defined as

$$\text{rmse} = \sqrt{\frac{1}{4}\left(\frac{1}{40}\right)\sum_{\lambda=1}^{4}\sum_{\theta=1}^{40}[L_p^{\text{obs}}(\theta, \lambda) - L_p^{\text{calc}}(\theta, \lambda)]^2}$$

$$= \sqrt{\frac{1}{4}\left(\frac{1}{40}\right)\sum_{\lambda=1}^{4}\sum_{\theta=1}^{40}[\omega_\lambda^{\text{obs}}\tau_\lambda^{\text{obs}}P_\lambda^{\text{obs}}(\theta) - \omega_\lambda^{\text{calc}}\tau_\lambda^{\text{calc}}P_\lambda^{\text{calc}}(\theta)]^2} \tag{4}$$

where the summation is over the wavelengths 440, 550, 670, and 870 nm and angles 1°–40° in 1° increments. The variable

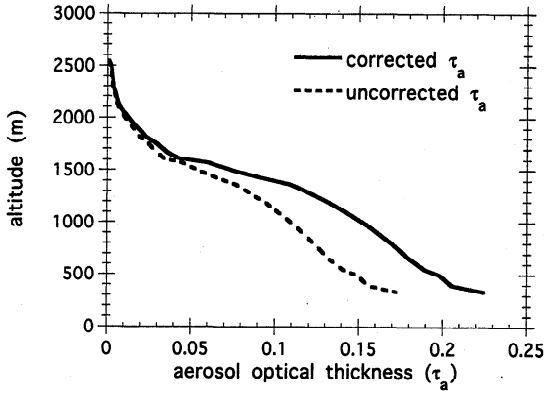

Figure 4. Example of humidity correction on aerosol optical thickness at 450 nm derived from vertical integration of σ_{sp}. Dashed curve shows τ_a from dry, uncorrected measurements. Solid curve shows τ_a with correction to ambient relative humidity ($\gamma = 0.35$). Vertical profile was taken on July 28 and corresponds to the data of Figure 1.

ω_λ is the single-scattering albedo, τ_λ is the optical thickness, and $P_\lambda(\theta)$ is the phase function for wavelength λ and angle θ. The look-up table includes lognormals in increments of $\Delta r_g = 0.03$ μm and $\Delta\sigma = 0.10$. The rms error for the case shown in Figure 3 was 8%. All rms errors in the look-up table matchups used in this study were 5–11%. The procedure does not require a unique solution. However, in most cases the match is unique with the rms error, often doubling for lognormals with particle size only 0.03 μm larger or smaller. In a few cases, two solutions were found with rms errors less than 11%. In those cases the lognormal producing the smallest rms error was selected.

4. Aerosol Optical Thickness

During SCAR-A the C-131A made a number of vertical profiles in cloud free air masses. These profiles spanned vertical layers of variable thicknesses (600–2200 m) in the lower troposphere and reached altitudes of 2500 m. After humidity correction the values of the aerosol scattering coefficient are vertically integrated over the vertical layers flown by the aircraft to determine the aerosol optical thickness in that atmospheric layer. The aerosol optical thickness from in situ measurements is given by

$$\tau_{\lambda,\text{scatt}} = \int_{Z_1}^{Z_2} \sigma_{sp}(z, \lambda)\, dz \tag{5}$$

where Z_2 and Z_1 define the top and bottom of the layer of interest, z is the altitude, and $\sigma_{sp}(z, \lambda)$ is the ambient aerosol scattering coefficient. This formula assumes only a vertical dependence of $\sigma_{sp}(z, \lambda)$. The vertical profiles measured by the aircraft are based, in general, on spiraling ascents or descents by the aircraft with the aircraft turn as tight as possible to achieve reasonable spatial resolution. However, this was not always the case nor was the aircraft profile always directly over a radiometer. Hence such profiles represent spatial averages over variable horizontal scales.

An example of the nephelometer integrated aerosol optical thickness (equation (5)) is shown in Figure 4 for a vertical profile flown on July 28. These data correspond to the σ_{sp} data of Figure 1. The variable τ_a is calculated for both the dry, uncorrected profile of σ_{sp} and the wet, corrected to ambient relative humidity profile of σ_{sp}. Note that the humidity correction results in an increase in optical thickness of 0.05. Also note that the nephelometer integrated aerosol optical thickness goes to zero at the top of the vertical profile. Aerosol above the integrating layer will not be included in the integration nor will aerosol located below the integrating layer be included.

The nephelometer aerosol optical thickness (equation (5)) for a wavelength of 450 nm along with the absorption optical thickness estimated from absorption photometer data and the total (i.e., absorption + scattering) optical depths measured by the closest ground-based radiometer at wavelength of 440 nm are shown in Table 1. Very few absorption measurements were available per sounding, and the corresponding aerosol optical thickness measurements in Table 1 are only indicative of the presence of relatively low absorption in the aerosol layers. Soundings 1 and 8 are the only two profiles which include aerosol near the ground.

One of the most difficult tasks in this procedure is the coordination in time and space of the in situ measurements with the surface array of radiometers. In Table 1 the in situ and

Table 1. Aerosol Optical Thickness From Integration of in Situ Measurements of Scattering τ_{sc} and Absorption τ_{ab} at 450 nm and From Simultaneous Measurements From Ground-Based Sun Radiometers τ_{rad} at 440 nm

Soundings	Date	Time	τ_{sc}	τ_{ab}	τ_{rad}	%	ω	Δz, m	z, m	km	Direction	Site
1	July 12	1033	0.3695	0.0005	0.76	49	0.9985	1510	0	31	SW	Wa
2	July 20	1303	0.4450	0.0030	0.76	59	0.9803	520	50	12	NE	Wa
3		1339	0.1621	0.0010	0.81	20	0.9914	−1100	650	55	SE	Co
4		1543	0.1897	0.0050	0.82	24	0.9885	−1280	420	13	NE	Wa
5	July 28	0826	0.2246	···	0.24	92	···	2350	290	75	SW	Wa
					0.44	51				50	NE	Ha
6		0900	0.1788	···	0.42	43	···	1790	930	30	S	Ha
7	July 28	1033	0.2134	···	0.40	54	···	2100	0	46	NE	Ha
8		1222	0.2113	···	0.37	56	···	−1580	520	30	S	Ha
9		1346	0.1383	···	0.30	45	···	−1950	280	11	SW	Ho

Also shown are the percentages of τ_{rad} explained by the in situ measurements, the single-scattering albedo ω, the thickness of the vertical profile with negative values indicating a descending sounding Δz, the minimum altitude during the sounding z, and the horizontal mean distance (km) and direction (dir) from the closest ground radiometer. The site is the name of the ground station: Wa, Wallops; Ha, Hampton Roads; Co, Coyle; Ho, Hog Island.

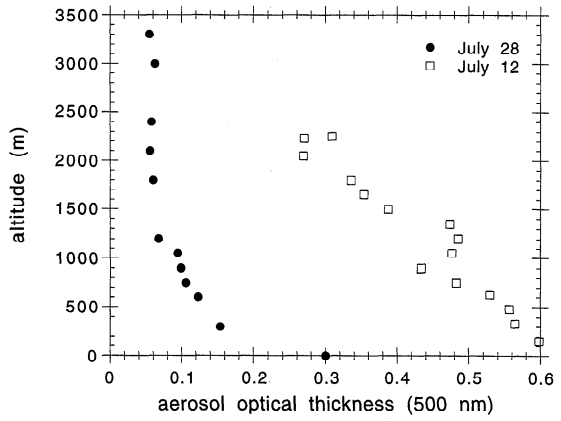

Figure 5. Aerosol optical thickness profiles from handheld Sun photometer data, carried aloft by light aircraft on July 12 (squares) and July 28 (dots). Each measurement represents aerosol optical thickness at 500 nm, existing above the aircraft at the time of measurement.

radiometer data are simultaneous in time and relatively close to each other spatially. Nevertheless, horizontal variability will influence the results of the comparison. A good example of this horizontal variability is shown in sounding 6 in which the plane flew between two ground-based radiometers while the optical thickness measured by these ground instruments differed significantly. At the bottom of the sounding the plane was located 44 km southwest from the Wallops ground station and 120 km northeast of the radiometer at Hampton Roads. At the top of the sounding the plane had flown 90 km to the southwest and was within 38 km of Hampton Roads, thereby perhaps starting and ending the profile in very different aerosol regimes. The distances listed in Table 1 refer to the average distance between the plane and the radiometer during the profile. A further complication is that during the time of the profile both radiometers were pointing eastward. The Hampton Roads radiometer pointed toward the plane's sample area, which covered a region of mixed inland and marine aerosols. The Wallops instrument, on the other hand, located to the northeast of the plane was pointing away from the plane's sample area and observing mostly offshore marine aerosol.

The in situ scattering optical thicknesses account on average for only 46% of the extinction aerosol optical thickness from the radiometers. Neither stratospheric aerosol estimated from stratospheric aerosol and gas experiment II data and other sources (τ_a = 0.01–0.03) [*Russell et al.*, 1996] nor the extension of the aerosol scattering coefficient with a decreasing exponential function (increasing τ_a by 0.0–0.06) are high enough to make up the difference between in situ and radiometer aerosol optical thicknesses.

Although direct measurements in the middle and high troposphere were not available in this experiment, it is possible that aerosols are present in the upper layers. This is suggested by the wind profiles obtained from soundings of local meteorological stations. The winds were predominately from the heavily polluted continent (west-northwest) at 0800 local time (LT) for all soundings listed in Table 1 and could easily have transported aerosols to the SCAR-A area in the layers above the extent of the C-131A's vertical profiles. In a previous experiment over the Chesapeake Bay an aerosol layer was encountered at approximately 3 km and continued above the aircraft's maximum height at 4.2 km [*Kaufman et al.*, 1986; *Ferrare et al.*, 1990]. Other experiments have observed aerosol layers above 4 km [*Kobayashi and Yano*, 1982; *Clarke et al.*, 1996]. This suggests that the characterization of aerosol extinction in this region requires in situ measurements that cover the vertical region from the ground to the middle troposphere. This hypothesis is corroborated by data taken from a light aircraft carrying a handheld Sun photometer on July 12 (1130 LT) and 28 (1145 LT). The light aircraft made vertical soundings of aerosol optical depth above the aircraft. The July 12 data were collected several hundred kilometers to the north of the in situ sample area but in the same extremely hazy, stagnant air mass that covered the entire mid-Atlantic region at the time. The July 28 data were collected between the Hog Island and Hampton Roads radiometers, in the same general area sampled by the C-131A. The absolute calibration on the handheld Sun photometers varies in its accuracy ($\tau_a = \pm 0.08$ at its worst). Furthermore, the handheld instruments collect data at 500 nm, while the in situ optical thicknesses are calculated at 450 nm, so comparison is inexact. However, qualitatively the data suggest that aerosol above the vertical profiles spanned by the C-131A is significant. These data are plotted in Figure 5. For example, on July 12 the measured optical thickness (λ = 500 nm) at 2200 m is 0.28–0.30. This indicates roughly half of the optical thickness measured at the ground remains above the light aircraft at 2200 m. If the same vertical profile holds for the area in which the C-131A made measurements up to 1510 m, then roughly 0.38 in optical thickness remained above the measurement range of the C-131A. This brings the percentage of the ground-based radiometer-measured optical thickness accounted for by the in situ method close to 100%.

Unsampled aerosol layers aloft are a possible explanation for the discrepancies in Table 1. Lidar data would give a definitive answer to the question, but no lidar data are available for SCAR-A. The theory of high-altitude aerosol layers is supported by previous studies and handheld Sun photometer data. However, until the C-131A or similarly equipped aircraft makes a complete profile from near ground to the middle troposphere, the results of the comparison between radiometer-derived and in situ measured optical thickness remains encouraging but inconclusive.

5. Aerosol Volume Size Distribution

5.1. Comparison of Individual Events

The C-131A aircraft measured size distributions during eight flights for 7 days during the SCAR-A experiment. Two of the C-131A flights were on cloudy days in which very little Sun/sky radiometer data were available. Typically, the C-131A flew 4–5 hour missions during midday. The Sun/sky radiometers, although collecting direct sun measurements every 15 min all day, made almucantar measurements only before 1030 (LT) and after 1600 (LT). Thus aerosol volume size distributions derived from the radiometer data are available only in the morning and late afternoon, usually before or after a C-131A flight. We identified nine events in which the C-131A made measurements of aerosol size distribution "close" (within 6 hours, 30 km, and 0.04 optical thickness) in time and space to a Sun/sky radiometer volume size distribution retrieval. These nine events are listed in Table 2.

The *Nakajima et al.* [1983, 1986] inversion algorithm produces volume size distributions integrated on the atmospheric column ($\mu m^3/cm^2$). The in situ measurements result in number

Table 2. Events in Which the C-131A Collected in Situ Data Within 30 km, 6 hours, and 0.04 Optical Thickness of a Ground-Based Radiometer Measuring Sky Radiance That Was Inverted Into Aerosol Volume Size Distribution

Event	Date	Time of Radiometer Observation	Time of in Situ Observation	τ_a 670 at Time of Radiometer	τ_a 670 at Time of in Situ	Heights of in Situ Observation
1	July 12	1009	1030–1130	0.40	0.42	0–1300 m
			1333–1346			
2	July 14	1009	1413–1422	0.44	0.40	500 m
		1009		0.38		
3	July 16	1009	1052–1107	0.13	0.14	200–500 m
4	July 16	1004	1145–1215	0.09	0.09	500 m
5	July 16	1009	1353–1407	0.13	0.13	800–1850 m
6	July 28	1010	0838–0852	0.14	0.13	1700–2500 m
7	July 28	1613	1038–1058	0.15	0.18	0–2100 m
8	July 28	1613	1058–1200	0.15	0.18	1500–750 m
9	July 28	1610	1353–1406	0.16	0.16	800 m
		1710		0.13		

In some cases, more than 1 measurement interval is considered in the event. The τ_a 670 is calculated from the radiometer direct Sun measurements, both at the time of the radiometer sky measurements and at the time of the in situ measurements. All times are in local time. On July 14 the C-131A took observations midway between two radiometers located 50 km apart.

size distributions which are easily converted to volume size distribution, assuming spherical particles. The in situ measurements are in units of true concentration, $\mu m^3/cm^3$. In order to compare the data, we assume an aerosol scale height of 1.5 km and convert the radiometer-derived size distribution to the concentration units. Furthermore, in 1993 an aerosol mode centered at a radius of 0.55 μm and representing approximately 0.03 of the aerosol optical thickness at 670 nm was discerned in the retrieved Sun/sky radiometer size distributions. This mode is the contribution of the stratospheric aerosol resulting from the 1991 Pinatubo eruption and is located far above the C-131A operation. In order to compare the data the stratospheric aerosol mode is removed from the radiometer-derived volume size distribution for all subsequent analyses. Four of the nine events are shown in Figure 6. The top two panels show data collected in hazy conditions. The bottom two panels show data in clearer conditions. Note the different vertical scale between the plots in hazy conditions and clear conditions. The heavier curves represent volume size distribution retrieved from the radiometers. The thinner curves are volume size distributions measured by the in situ instrumentation with thin solid lines representing no-bag samples and thin broken lines representing PCASP data. All the data plotted in the same panel were collected when the aircraft was close in time, space, and optical thickness to the almucantar retrieval.

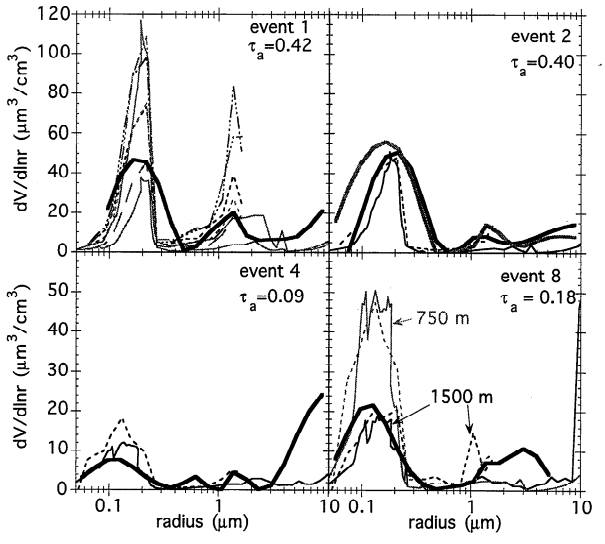

Figure 6. Comparison of aerosol volume size distribution from in situ no-bag data (thin solid curves), in situ passive cavity aerosol spectrometer probe (PCASP) measured data (thin-dashed curves), and inferred radiometer data (thick curves) for individual events when the in situ measurements were taken close in time, space, and aerosol conditions to the radiometer measurements (Table 2). For the in situ data, lines of similar tone were observed at the same altitude.

The four panels of Figure 6 illustrate the typical characteristics of all nine events. Looking at the in situ data independently, we see that there is a large amount of variability in the total volume of particles but less variability in the size distribution of the volume. The variability in total volume is caused primarily by horizontal or vertical spatial variability. For example, the thin gray curves of event 8 in Figure 6 represent aerosol characteristics as collected at 750 m, while the thin black curves represent data collected in the same location, 30 min later, but at 1500 m. There is also variability between in situ instruments. The no-bag data (thin solid curves) show consistently lower concentrations of aerosol volume for large particles than does the wing-mounted PCASP probe (thin broken curves). The no-bag data are expected to lose large-particle volume before the concentration is measured because the large particles are the first to settle in the bag and impact on the sample lines in the measurement system. The PCASP probe is the preferred in situ device to measure large-particle volume. Unfortunately, the PCASP probe measures data only to a radius of 1.5 μm. Thus comparisons between the in situ measurements and the remotely sensed measurements at particles with radii >1.5 μm are impossible. Nonetheless, we can make good comparisons for accumulation mode particles and for coarse mode particles in the 1–2 μm range, although the comparison is affected by the spatial and temporal variability in the data.

Figure 7 compares the in situ data for event 1 on July 12 for

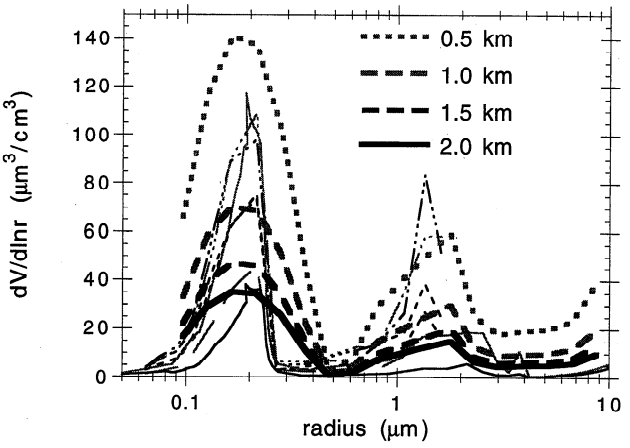

Figure 7. Aerosol volume size distribution for event 1 on July 12. Data from in situ instruments are plotted as thin curves. Data derived from radiometer sky measurements are plotted as thick curves. Shown are the different size distributions resulting from the same sky radiance but assuming different aerosol-scale heights ranging from 0.5 km (gray dotted curve) to 2.0 km (solid curve). In all other plots and analyses a well-mixed boundary layer of 1.5 km is assumed.

a variety of assumptions of aerosol scale height. We see that for reasonable assumptions of aerosol scale height the radiometer-derived data can be "fine-tuned" for each event to better agree with the in situ data. We refrain from this fine-tuning in order to maintain consistency and instead, retain a uniform scale height of 1.5 km for all nine events. This value may not be exact in each case but does give overall reasonable values. The scale height assumption clearly affects the magnitude of the total volume but does not affect the radii and relative sizes of the modes. The radiometer-derived distributions locate the accumulation mode between 0.1 and 0.2 μm and a coarse mode between 1 and 2 μm. The radiometer-derived data agree with the in situ data in the placement of the modes. Agreement is best for the accumulation mode and less accurate for the coarse mode. However, when the coarse mode is prevalent in the in situ data (event 1) it is also well represented in the radiometer data. Thus we conclude that the volume size distributions inverted from the sky radiance measurements do represent the same quantity measured close in time and space by airborne in situ instruments.

5.2. Comparison of Trends

Figure 8 shows the accumulation mode volume-weighted mean radius r_v plotted against aerosol optical thickness at 670 nm, where r_v is defined as

$$r_v = \int_0^{0.50} r \frac{dV}{dr}\, dr \Big/ \int_0^{0.50} \frac{dV}{dr}\, dr \qquad (6)$$

where r is the radius and dV/dr is the volume size distribution. The limits of integration refer to the size range of the accumulation mode. The upper limit of 0.50 μm was chosen to separate accumulation mode volume from coarse mode volume, generally, the point of local minimum in the volume distribution curves. Figure 8 shows the radiometer-derived values, the no-bag values, and the PCASP sampled values. Table 3 lists the values plotted in Figure 8. All three instruments show the mean radius of the accumulation mode increasing, as optical thickness increases. This is a trend apparent not only in these nine comparison events but in the larger SCAR-A radiometer database which spans more than 2 months and incorporates over 125 symmetrical almucantars [*Remer et al.*, 1996]. The two airborne instrument methods give roughly the same r_v, while the radiometer-derived method gives an r_v systematically 0.01–0.02 μm (approximately 10%) larger. The reason for this discrepancy will become apparent when we compare the trends in accumulation mode widths. Linear regression equations and correlation coefficients are given in Table 4.

Table 3 also lists values of the ratio between the accumulation mode volume and the coarse mode volume. The ratio ranges from 3.3 to 13.6 for the radiometer-derived data and from 1.4 to 10.5 for the PCASP data. The coarse mode is not well measured by the no-bag instruments and is not included. Measurements of PCASP volume ratio fluctuate greatly even on the same flight. This, in general, is due to variability of the coarse mode measurements, although it is unclear whether the variability is an instrument artifact or simply the nature of coarse mode particles which are spatially less homogeneous than accumulation mode particles.

Figure 8 also shows the accumulation mode width σ as a function of aerosol optical thickness at 670 nm. The accumulation mode width σ is defined as the standard deviation of the natural logarithm of the radius given by

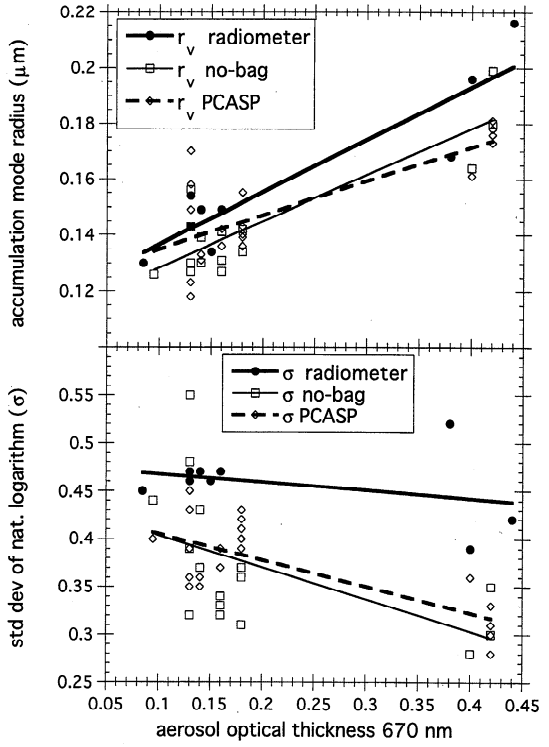

Figure 8. (top) Volume-weighted mean accumulation mode radius r_v and (bottom) standard deviation of the natural logarithm of the radius σ derived from radiometer data (dots), in situ no-bag data (squares), and PCASP data (diamonds) as a function of aerosol optical thickness at 670 nm, τ_{670}. The τ_{670} is calculated from radiometer sun measurements. The r_v and σ are plotted for each retrieved size distribution occurring during the nine comparison events. Also shown are the linear regression lines fitting each sample. The data for the plot are listed in Table 3. Regression equations are given in Table 4.

Table 3. Volume-Weighted Accumulation Mode Radius r_v, Standard Deviation of the Natural Logarithm of the Radius in the Accumulation Mode σ, and Ratio Between Volume of Accumulation Mode and Volume of Coarse Mode for Each of the Volume Size Distributions Compared

	r_v			σ			Ratio	Ratio
Event	Radiometer	No-Bag	PCASP	Radiometer	No-Bag	PCASP	Radiometer	PCASP
1	0.196	0.180	0.176	0.39	0.35	0.31	3.3	1.7
		0.199	0.173		0.30	0.31		3.0
			0.173			0.33		2.1
			0.178			0.30		2.4
			0.181			0.28		1.8
			0.159			0.36		2.2
2	0.216	0.164	0.161	0.42	0.28	0.36	9.4	7.1
	0.168			0.52			13.6	
3	0.154	0.130	0.133	0.47	0.43	0.35	8.0	5.8
		0.139	0.131		0.37	0.36		4.6
4	0.130	0.126	0.135	0.45	0.44	0.40	3.7	5.4
5	0.154	0.130	0.149	0.47	0.55	0.45	8.0	1.8
		0.143	0.170		0.48	0.36		9.6
			0.158			0.43		1.4
6	0.149	0.156	0.123	0.47	0.39	0.39	8.3	7.0
		0.127	0.143		0.32	0.39		7.2
			0.118			0.35		10.0
7	0.134	0.142	0.139	0.46	0.36	0.40	8.4	6.2
			0.140			0.41		9.6
			0.143			0.43		3.4
8	0.134	0.142	0.155	0.46	0.37	0.42	8.4	3.7
		0.134	0.136		0.31	0.39		10.5
9	0.149	0.141	0.142	0.47	0.33	0.39	4.8	6.8
	0.143	0.127	0.136	0.46	0.32	0.37	4.5	7.9
		0.131	0.142		0.34	0.39		5.2

Times of events are listed in Table 2. Four of the nine events are plotted in Figure 6. The values of r_v and σ are plotted against optical thickness in Figure 8. The in situ measurements include both the no-bag and passive cavity aerosol spectrometer probe (PCASP) measured volume size distributions, except for the ratio which includes only the PCASP data.

$$\sigma = 1/V \sqrt{\sum \ln (r/r_v)^2} \quad (7)$$

where V is the total volume of the accumulation mode in the volume size distribution, r is the radius, and r_v is the volume-weighted mean mode radius. There is an apparent trend in the in situ instruments that shows that σ decreases with optical thickness. However, there is much scatter in the data and correlation coefficients are low (Table 4). The significance of Figure 8 is that the two airborne instrument systems give very similar values of σ, while the radiometer-derived values are consistently higher, especially for higher optical thickness. Looking back at Figure 6, we see qualitatively what Figure 8 shows quantitatively. The in situ data reveal that the mode, especially the accumulation mode, is not a smooth curve. The abruptness of the cutoff of the accumulation mode at radius 0.3 μm is found in other in situ and theoretical studies [*Hoppel et al.*, 1990; *Kaufman and Tanré*, 1994]. The inversion technique demands smoothly fitted curves. It cannot resolve the abrupt cutoff found in the direct measurements of the in situ data. The result is that the inversion produces broader smoother curves, which have a larger σ. The smoothly fitted inversion curve produces a 5–10% larger mean radius (r_v) than the abruptly ending in situ curve because the in situ curve has relatively little "weight" given to the larger radii of the accumulation mode. Figure 8 illustrates one of the disadvantages of inferring aerosol physical properties from optical ones. The assumptions and mathematical limitations of the numerical inversion prevent the retrieval of sharply defined modes in the size distribution. Without the corresponding in situ data we would not have been aware of the actual shape to the accumulation mode, the abrupt cutoff, and the resulting effect on r_v and σ.

Table 4. Linear Regression Equations and Correlation Coefficients Relating the r_v and σ of the Natural Logarithm of the Radius in the Accumulation Mode to Aerosol Optical Thickness at 670 nm, τ_{670}

Equation	System	Coefficient
$r_v = 0.118 + 0.189 \times \tau_{670}$	radiometer	0.906
$r_v = 0.116 + 0.167 \times \tau_{670}$	no bag	0.880
$r_v = 0.123 + 0.121 \times \tau_{670}$	PCASP	0.798
$\sigma = 0.475 - 0.083 \times \tau_{670}$	radiometer	0.330
$\sigma = 0.438 - 0.336 \times \tau_{670}$	no bag	0.512
$\sigma = 0.433 - 0.277 \times \tau_{670}$	PCASP	0.755

Shown are the separate values for radiometer-derived data, no-bag data, and PCASP data.

6. Discussion and Conclusions

The primary advantage of airborne in situ instrumentation is that these instruments directly measure the volume aerosol properties such as concentration, size distribution, cloud condensation nuclei concentration, and scattering coefficient. However, total column aerosol optical properties, such as aerosol optical thickness, must be inferred from the locally measured data, and assumptions must be made. None of the in

situ instruments measure the ambient aerosol. The instruments which rely on bag samples of the aerosol are the worst offenders. The relative humidity in the bag environment is kept at 40%, while the ambient conditions can be over 90%. The PCASP probe mounted on the wing comes closest to ambient conditions, but even it dries the aerosol in the measurement process. There are also inadvertent size sorting effects by the intake apparatus on the in situ instruments. Larger particles are more susceptable to impaction and sedimentation than smaller particles. This creates errors in particle concentration of the larger particles and errors in size distribution [*Huebert et al.*, 1990]. Furthermore, the aircraft must be airborne in order to make measurements, and therefore observations are a relatively rare event.

The advantages of the Sun/sky radiometers are that they make a direct measure of the total column optical properties of the ambient aerosol unchanged by sampling efficiency and drying and that these automatic instruments, once deployed, collect data every 15 min (direct Sun measurements) or every hour (sky radiance measurements) from sunrise to sunset, day after day. These instruments produce an aerosol climatology impossible to duplicate by the temporally sparse data collected by the airborne in situ instrumentation. However, the Sun/sky radiometer data are not without drawbacks. First, there is a sampling bias to the aerosol climatology produced. Sky radiance cannot be collected on cloudy days. The days in which aerosol-cloud interaction is prevalent will be underrepresented in the database. Furthermore, aerosol physical properties from remote sensing data must be retrieved through inversion techniques, while in situ instrumentation measures these quantities directly. All inversion techniques are subject to the validity of their assumptions. In order to retrieve size distribution from the sky radiance we have had to make assumptions concerning particle sphericity, refractive index, surface reflectance, sky homogeneity, and lognormal distribution of small accumulation mode particles. Inversion techniques are also sometimes sensitive to errors in calibration, measurement of angle or stray light.

The two measurement techniques measure different quantities which must be adjusted or inverted in order to be compared; therefore neither is a validation of the other. However, we find that after carefully matching observation events there is agreement in measurements of aerosol volume size distribution and the depiction of the dynamic nature of the accumulation mode aerosol as it increases in radius with increasing optical thickness. The comparison of aerosol optical thickness is less conclusive without lidar data or in situ measurements that sample into the middle troposphere. However, the present analysis coupled with previous experiments that did sample at higher altitudes and an independent measure of aerosol optical thickness aloft suggest agreement is possible. The agreement we find between the two instruments in actual field conditions is encouraging and suggests that the assumptions and adjustments made are indeed correct. The interesting results of this study concern the areas in which the measurements do not agree. For the optical thickness comparison the major disagreement can be explained by the existence of aerosol layers aloft which remain unobserved by the C-131A's normal vertical profile. In future field campaigns, in situ measurements of aerosol at altitudes greater than 2 km and lidar data will be necessary to achieve a true closure. For the aerosol volume size distribution comparison, even though the methods produce qualitatively similar distributions peaked at the same modal radius, the inverted sky radiance data cannot resolve the sharp cutoff of the in situ measured distribution. The shape of the accumulation mode can be optically important and failure to model the shape of the size distribution correctly can result in significant errors for climate and satellite remote sensing applications.

Acknowledgments. We would like to thank Ilya Slutsker for creating the software and maintaining the database of Sun/sky radiometer data and Bo-Cai Gao, Richard Kleidman, Eric Vermote, and Jean-Claude Roger for installing and collecting Sun/sky radiometer data on the ground and in the light aircraft during SCAR-A.

References

Charlson, R. J., J. Langer, H. Rodhe, C. B. Leovy, and S. G. Warren, Perturbation of the northern hemispheric radiative balance by backscattering from anthropogenic sulfate aerosol, *Tellus*, *43*, 152–163, 1991.

Charlson, R. J., S. E. Schwartz, J. M. Hales, R. D. Cess, J. A. Coakley Jr., J. E. Hansen, and D. J. Hofmann, Climate forcing by anthropogenic aerosol, *Science*, *255*, 423–430, 1992.

Clarke, A. D., J. N. Porter, F. P. J. Valero, and P. Pilewskie, Vertical profiles, aerosol microphysics, and optical closure during the Atlantic Stratocumulus Transition Experiment: Measured and modeled column optical properties, *J. Geophys. Res.*, *101*, 4443–4453, 1996.

Covert, D. S., R. J. Charlson, and N. C. Ahlquist, A study of the relationship of chemical composition and humidity to light scattering by aerosols, *J. Appl. Meteorol.*, *11*, 968–976, 1972.

Dave, J. V., and J. Gazdag, A modified Fourier transform method for multiple scattering calculations in a plane parallel Mie atmosphere, *Appl. Opt.*, *9*, 1457–1466, 1970.

Durkee, P. A., F. Pfeil, E. Frost, and R. Shema, Global analysis of aerosol particle characteristics, *Atmos. Environ., Part A*, *25*, 2457–2471, 1991.

Ferrare, R. A., R. S. Fraser, and Y. J. Kaufman, Satellite measurements of large-scale air pollution: Measurements of forest fire smoke, *J. Geophys. Res.*, *95*, 9911–9925, 1990.

Hanel, G., The properties of atmospheric aerosol particles as functions of the relative humidity at thermodynamic equilibrium with the surrounding moist air, *Adv. Geophys.*, *19*, 73–188, 1976.

Hegg, D. A., R. J. Ferek, and P. V. Hobbs, Aerosol size distributions in the cloudy atmospheric boundary layer of the North Atlantic ocean, *J. Geophys. Res.*, *98*, 8841–8846, 1993a.

Hegg, D. A., R. J. Ferek, and P. V. Hobbs, Light scattering and cloud condensation nucleus activity of sulfate aerosol measured over the northeast Atlantic Ocean, *J. Geophys. Res.*, *98*, 14,887–14,894, 1993b.

Hegg, D. A., P. V. Hobbs, R. J. Ferek, and A. P. Waggoner, Measurements of some aerosol properties relevant to radiative forcing on the east coast of the United States, *J. Appl. Meteorol.*, *34*, 2306–2315, 1995.

Hegg, D. A., D. S. Covert, M. J. Rood, and P. V. Hobbs, Measurement of aerosol optical properties in marine air, *J. Geophys. Res.*, *101*, 12,893–12,903, 1996.

Hobbs, P. V., L. F. Radke, J. H. Lyons, R. J. Ferek, and D. J. Coffman, Airborne measurements of particle and gas emissions from the 1990 volcanic eruptions of Mount Redoubt, *J. Geophys. Res.*, *96*, 18,735–18,752, 1991.

Holben, B. N., E. Vermote, Y. J. Kaufman, D. Tanré, and V. Kalb, Aerosol retrieval over land from AVHRR data-application for atmospheric correction, *IEEE Trans. Geosci. and Remote Sens.*, *30*, 212–222, 1992.

Holben, B. N., A. Setzer, T. F. Eck, A. Pereira, and I. Slutsker, Temporal and spatial variability of aerosol loading and properties during the Amazon Basin dry season, 1992–1994, *Remote Sens. Environ.*, in press, 1996.

Hoppel, W. A., J. W. Fitzgerald, and R. E. Larson, Aerosol size distributions in air masses advecting off the east coast of the United States, *J. Geophys. Res.*, *90*, 2365–2379, 1985.

Hoppel, W. A., J. W. Fitzgerald, G. M. Frick, R. E. Larson, and E. J. Mack, Aerosol size distributions and optical properties found in the marine boundary layer over the Atlantic Ocean, *J. Geophys. Res.*, *95*, 3659–3686, 1990.

Huebert, B. J., G. Lee, and W. L. Warren, Airborne aerosol inlet

passing efficiency measurement, *J. Geophys. Res.*, *95*, 16,369–16,381, 1990.

Husar, R. B., J. M. Holloway, and D. E. Patterson, Spatial and temporal pattern of eastern U.S. haziness: A summary, *Atmos. Environ.*, *15*, 1919–1928, 1981.

Intergovernmental Panel on Climate Control, Radiative forcing of climate change, *Clim. Change*, 339 pp., 1994.

Kaufman, Y. J., and R. S. Fraser, Light extinction by aerosols during summer air pollution, *J. Clim. Appl. Meteorol.*, *22*, 1694–1706, 1983.

Kaufman, Y. J., and B. N. Holben, Hemispherical backscattering by biomass burning and sulfate particles derived from sky measurements, *J. Geophys. Res.*, *101*, 19,433–19,445, 1996.

Kaufman, Y. J., and D. Tanré, Effect of variations in supersaturation on the formation of cloud condensation nuclei, *Nature*, *369*, 45–48, 1994.

Kaufman, Y. J., T. W. Brakke, and E. W. Eloranta, Field experiment to measure the radiation characteristics of a hazy atmosphere, *J. Atmos. Sci.*, *43*, 1135–1151, 1986.

Kaufman, Y. J., A. Gitelson, A. Karnieli, E. Ganor, R. S. Fraser, T. Nakajima, S. Mattoo, and B. N. Holben, Size distribution and scattering phase function of aerosol particles retrieved from sky brightness measurements, *J. Geophys. Res.*, *99*, 10,341–10,356, 1994.

Kiehl, J. T., and B. P. Briegleb, The relative roles of sulphate aerosols and greenhouse gases in climate forcing, *Science*, *260*, 311–314, 1993.

King, M. D., D. M. Byrne, B. M. Herman, and J. A. Reagan, Aerosol size distributions obtained by inversion of spectral optical depth measurements, *J. Atmos. Sci.*, *35*, 2153–2167, 1978.

Kobayashi, T., and N. Yano, Relation between observed aerosol thickness and calculated values from size distribution measurements, *J. Meteorol. Soc. Jpn.*, *60*, 1249–1258, 1982.

Leaitch, W. R., G. A. Isaac, J. W. Strapp, C. M. Banic, and H. A. Wiebe, The relationship between cloud droplet number concentrations and anthropogenic pollution: Observations and climatic implications, *J. Geophys. Res.*, *97*, 2463–2474, 1992.

Liu, P. S. K., W. R. Leaitch, J. W. Strapp, and M. A. Waseg, Response of particle measuring systems Airborne ASASP and PCASP to NaCl and latex particles, *Aerosol Sci. Technol.*, *16*, 83–95, 1992.

McMurry, P. H., and M. R. Stolzenburg, On the sensitivity of particle size to relative humidity for Los Angeles aerosols, *Atmos. Environ.*, *23*, 497–507, 1989.

Mitchell, J. F. B., T. C. Johns, J. M. Gregory, and S. F. B. Tett, Climate response to increasing levels of greenhouse gases and sulphate aerosols, *Nature*, *376*, 501–504, 1995.

Nakajima, T., M. Tanaka, and T. Yamauchi, Retrieval of the optical properties of aerosols from aereole and extinction data, *Appl. Opt.*, *22*, 2951–2959, 1983.

Nakajima, T., M. Takamura, M. Yamano, M. Shiobara, T. Yamauchi, R. Goto, and K. Murai, Consistency of aerosol size distribution inferred from measurements of solar radiation and aureole, *J. Meteorol. Soc. Jpn.*, *64*, 765–776, 1986.

Radke, L. F., Preliminary measurements of the size distribution of cloud interstitial aerosol in, *Precipitation Scavenging, Dry Deposition and Resuspension*, edited by H. R. Pruppacher, R. G. Semonin, and W. S. N. Slinn, pp. 71–78, Elsevier, New York, 1983.

Remer, L. A., Y. J. Kaufman, and B. N. Holben, The size distribution of ambient aerosol particles: Smoke vs. urban/industrial aerosol, in *Chapman Conference on Biomass Burning*, edited by J. Levine, MIT Press, Cambridge, Mass., in press, 1996.

Russell, P. B., et al., Global to microscale evolution of the Pinatubo volcanic aerosol, derived from diverse measurements and analyses, *J. Geophys. Res.*, *101*, 18,745–18,763, 1996.

Svenningson, I. B., H.-C. Hansson, A. Wiedensohler, J. A. Ogren, K. J. Noone, and A. Hallberg, Hygroscopic growth of aerosol particles in the Po Valley, *Tellus*, *Ser. B*, *44*, 556–569, 1992.

Twomey, S. A., The influence of pollution on the shortwave albedo of clouds, *J. Atmos. Sci.*, *34*, 1149–1152, 1977.

Twomey, S. A., M. Piepgrass, and T. L. Wolfe, An assessment of the impact of pollution on global cloud albedo, *Tellus*, *Ser. B*, *36*, 356–366, 1984.

Van de Hulst, H. C., *Light Scattering by Small Particles*, Dover, Mineola, N. Y., 1957.

Weiss, R. E., and A. P. Waggoner, Aerosol optical absorption: Accuracy of filter measurement by comparison with in-situ extinction, in *Aerosols*, edited by P. Y. H. Liu, D. Y. H. Pui, and H. Frissar, pp. 397–400, Elsevier, New York, 1984.

Whitby, K. T., The physical characteristics of sulfur aerosols, *Atmos. Environ.*, *12*, 135–159, 1978.

Wiscombe, W. J., Mie scattering calculations—Advances in technique and fast, vector-speed computer codes, *NCAR Tech. Note TN-140+STR*, Natl. Cent. for Atmos. Res., Boulder, Colo., 1979.

Wiscombe, W. J., Improved Mie scattering algorithms, *Appl. Opt.*, *19*, 1505–1509, 1981.

S. Gasso and D. A. Hegg, Department of Atmospheric Science, University of Washington, Seattle, WA 98195.

B. N. Holben, Laboratory for Terrestrial Physics, Code 923, NASA Goddard Space Flight Center, Greenbelt, MD 20771.

Y. J. Kaufman, Laboratory for Atmospheres, Code 913, NASA Goddard Space Flight Center, Greenbelt, MD 20771.

L. A. Remer, Science Systems and Applications, Inc., Code 913, NASA Goddard Space Flight Center, Greenbelt, MD 20771. (e-mail: remer@climate.gsfc.nasa.gov)

(Received January 10, 1996; revised May 30, 1996; accepted May 30, 1996.)